

Collaborative filtering based on nonnegative/binary matrix factorization

Yukino Terui¹, Yuka Inoue¹, Yohei Hamakawa², Kosuke Tatsumura², and Kazue Kudo^{1,3,*}

¹Department of Computer Science, Ochanomizu University, Tokyo 112-8610, Japan

²Corporate Research and Development Center, Toshiba Corporation, Kawasaki 212-8582, Japan

³Graduate School of Information Sciences, Tohoku University, Sendai 980-8579, Japan

*kudo@is.ocha.ac.jp

ABSTRACT

Collaborative filtering generates recommendations based on user-item similarities through rating data, which may involve numerous unrated items. To predict scores for unrated items, matrix factorization techniques, such as nonnegative matrix factorization (NMF), are often employed to predict scores for unrated items. Nonnegative/binary matrix factorization (NBMF), which is an extension of NMF, approximates a nonnegative matrix as the product of nonnegative and binary matrices. Previous studies have employed NBMF for image analysis where the data were dense. In this paper, we propose a modified NBMF algorithm that can be applied to collaborative filtering where data are sparse. In the modified method, unrated elements in a rating matrix are masked, which improves the collaborative filtering performance. Utilizing a low-latency Ising machine in NBMF is advantageous in terms of the computation time, making the proposed method beneficial.

Introduction

Collaborative filtering is often applied in recommendation systems that primarily serve Internet services, such as e-commerce and video distribution platforms^{1,2}. The essence of collaborative filtering lies in generating personalized recommendations based on the intrinsic similarities between users and items. Collaborative filtering relies on training data, in which users assign scores or ratings to various items. As it is common for users to omit ratings of specific items, leading to missing data, the central objective of collaborative filtering is to predict the scores for unrated items. Matrix factorization techniques, particularly nonnegative matrix factorization (NMF)³, are frequently employed. When using NMF for collaborative filtering, the ranking matrix V , whose entries are nonnegative, is approximated as the product of two nonnegative matrices W and H , that is, $V \approx WH$. The standard approach involves minimizing the difference between V and WH . In the optimization procedure, each element of W and H is constrained to be nonnegative. While the multiplicative update algorithm is the most prevalent approach for NMF⁴, we focus on another technique known as the alternative nonnegative least-squares approach using the projected gradient method (PGM)⁵. The convergence of the alternative update method for NMF is shown in Ref. 5. Such an alternative optimization method is essential for solving nonnegative/binary matrix factorization (NBMF)^{6,7}, which is an extension of NMF. References 6, 7 used D-wave's quantum annealers to solve quadratic binary optimization problems involved in NBMF, and demonstrated a speedup compared with two classical solvers.

In recent years, Ising machines, initially designed to solve combinatorial optimization problems efficiently, have found new applications in the field of machine learning, expanding their scope beyond their original purpose⁶⁻¹⁴. Ising machines are special-purpose computers for solving combinatorial optimization problems, and are realized by several types of devices, such as quantum annealers¹⁵, digital processors based on simulated annealing¹⁶⁻²², digital processors based on simulated bifurcation (SB)²³⁻²⁶, and coherent Ising machines²⁷⁻³⁴. As Ising machines usually accept problems described by the Ising model or quadratic unconstrained binary optimization formulation, their application to machine learning requires hybrid methods that utilize both an Ising machine and a general-purpose computer (e.g., a CPU). In NBMF, the matrix elements of H are binary, whereas those of W are real and nonnegative. Therefore, an Ising machine is employed to accelerate the update of matrix H , whereas a general-purpose computer (e.g., a CPU) handles the update of matrix W . As the updates of matrices H and W are repeated alternately, NBMF inevitably involves a computation time overhead owing to the communication between the Ising machine and the CPU. The advantages and disadvantages of NMF (using a CPU) and NBMF (using a CPU and Ising machine) remain unclear in terms of solution quality, computation time, and applicability to sparse problems.

In this paper, we propose a novel approach for applying NBMF to collaborative filtering. Previous studies have employed NBMF for image analysis^{6,12,14} that deals with dense data matrices, where the majority of matrix elements have nonzero values. By contrast, collaborative filtering involves sparse data matrices, with most elements remaining undetermined. We propose a modified NBMF algorithm that masks undetermined elements within the data matrix to improve the prediction

accuracy. In addition, we compare NBMF with NMF in terms of the quality of the solution and computation time and investigate the dependency of the characteristics on the sparsity and size of the problem. To accelerate the NBMF algorithm, we used an SB-based machine implemented with a field-programmable gate array (FPGA)^{25,26} that supports up to 2,048 spins and has full spin-to-spin connectivity (no need for minor embedding techniques required for local-connectivity Ising machines^{6,7,12,14}). Incorporating an SB-based machine to update the binary matrix elements yields a substantial reduction in the overall computational time required for NBMF compared with NMF. Furthermore, the low-latency characteristic of the SB-based machine²⁶ (no need for network access) is advantageous for executing the iterative method using a general-purpose computer (a CPU) and Ising machine, alternatively, reducing the communication time between them. This study presents the first empirical evidence that NBMF, when implemented with a low-latency Ising machine, surpasses NMF in terms of both solution quality and overall computational efficiency.

Related work

There are different recommendation systems based on sparse data matrices. For example, the Top-N recommendation systems can be made effective through matrix completion with log-determinant regularization³⁵. Regularization also plays an important role in models based on latent factor analysis, which is efficient for recommendation systems. For example, elastic net regularization was proposed to achieve high prediction accuracy for missing data in Ref. 36.

Matrix factorization techniques, particularly NMF, are frequently employed to extract the features of high-dimensional data. Clustering using extracted data is a typical application of NMF, and various methods have been proposed. For example, the NMF method proposed in Ref. 37 learned local similarity and clustering in a mutually enhanced manner. NMF with log-norm regularization³⁸ enhances the sparseness of the extracted data, making clustering effective. The recently proposed deep learning clustering methods^{39–44} based on NMF outperformed competitive methods.

Although these studies are related to our work, their purposes are different from ours. This study aims to demonstrate the advantages of the low-latency Ising machine, and a comparison with recent methods of NMF is beyond the scope of this study. Since our NBMF approach uses both a CPU and a low-latency Ising machine, comparing it with NMF is vital to accurately assess the hybrid system's efficiency. Thus, our focus is on the computational efficiency but not on recommendation systems.

Models and algorithms

Nonnegative/binary matrix factorization

NBMF decomposes a nonnegative $n \times m$ matrix V into a nonnegative $n \times k$ matrix W and a binary $k \times m$ matrix H :

$$V \approx WH. \quad (1)$$

The approach to conducting factorization involves minimizing $\|V - WH\|_F$, where the Frobenius norm is defined as $\|A\|_F = \sqrt{\sum_{i,j} A_{ij}^2}$ and A_{ij} is the (i, j) element of A . To achieve minimization, NBMF employs an iterative alternative update procedure as follows:

$$W = \arg \min_{X \in \mathbb{R}_+^{n \times k}} (\|V - XH\|_F^2 + \lambda_1 \|X\|_F^2), \quad (2)$$

$$H = \arg \min_{X \in \{0,1\}^{k \times m}} (\|V - WX\|_F^2 + \lambda_2 \|X\|_F^2), \quad (3)$$

where X is a matrix that corresponds to W and H in Eqs. 2 and 3, respectively. Hyperparameters λ_1 and λ_2 are positive.

The matrix W is updated row-by-row. The objective function for the row vector \mathbf{x}^\top of W is given by

$$f_W(\mathbf{x}) = \frac{1}{2} \|\mathbf{v} - H^\top \mathbf{x}\|^2 + \frac{\lambda_1}{2} \|\mathbf{x}\|^2, \quad (4)$$

where \mathbf{v}^\top is the corresponding row vector in matrix V . We applied the PGM to minimize the objective function for each row vector, as detailed in the Methods section. The PGM was executed using a general-purpose computer. In contrast, matrix H is updated column-by-column. The objective function for optimizing the column vector \mathbf{q} ($\in \{0, 1\}^k$) of H is given by

$$f_H(\mathbf{q}) = \frac{1}{2} \|\mathbf{u} - W\mathbf{q}\|^2 + \frac{\lambda_2}{2} \|\mathbf{q}\|^2, \quad (5)$$

where \mathbf{u} is the corresponding column vector in matrix V . To minimize the objective function for each column, we employed an SB-based Ising machine²⁶, as Eq. (5) can be reformulated in the Ising model form (refer to the Model section for details).

In this study, we compared NMF and NBMF. In NMF, Eqs. (2) and (3) are also used; however, $X \in \{0, 1\}^{k \times m}$ in Eq. (3) is substituted by $X \in \mathbb{R}_+^{k \times m}$. Furthermore, each column vector \mathbf{q} in Eq. (5) should be nonnegative. Equations (4) and (5) were minimized using the PGM in NMF, and the computation was executed on a general-purpose processor (a CPU).

Collaborative filtering

In the context of collaborative filtering, matrix V is a rating matrix, where the (i, j) element v_{ij} represents the user i 's rating of item j . As the rating matrix is generally sparse, the treatment of unrated entries significantly influences the collaborative filtering performance. A straightforward approach is to assign a rating of zero to unrated entries, which is a simple and practical choice. Another method for handling unrated entries is to introduce a mask matrix of the same size as matrix V after assigning them a zero rating. The elements of the mask matrix M are defined as follows:

$$M_{ij} = \begin{cases} 1 & (V_{ij} \neq 0), \\ 0 & (V_{ij} = 0). \end{cases} \quad (6)$$

For collaborative filtering, we propose a modified NBMF method in which the masked matrix is decomposed as

$$M \circ V \approx M \circ (WH), \quad (7)$$

where \circ denotes the Hadamard product $(M \circ V)_{ij} = M_{ij}V_{ij}$.

In the modified NBMF algorithm, the objective function for updating the matrix W , as defined by Eq. (4), is replaced with

$$f_W(\mathbf{x}) = \frac{1}{2} \|\tilde{\mathbf{v}} - \tilde{H}^\top \mathbf{x}\|^2 + \frac{\lambda_1}{2} \|\mathbf{x}\|^2. \quad (8)$$

When updating the i th row, the j th elements are given by $\tilde{v}_j = M_{ij}V_{ij}$ and $(\tilde{H}^\top \mathbf{x})_j = \sum_l M_{lj}H_{lj}x_l$. Similarly, the objective function for updating matrix H , as expressed in Eq. (5), is replaced by

$$f_H(\mathbf{q}) = \frac{1}{2} \|\tilde{\mathbf{u}} - \tilde{W}\mathbf{q}\|^2 + \frac{\lambda_2}{2} \|\mathbf{q}\|^2. \quad (9)$$

When updating the j th column, the i th element is given by $\tilde{u}_i = M_{ij}V_{ij}$, and $(\tilde{W}\mathbf{q})_i = \sum_l M_{il}W_{il}q_l$.

Results

For collaborative filtering based on NBMF and NMF, we used the MovieLens 1M dataset⁴⁵; Netflix prize data⁴⁶; Yahoo! music user ratings of songs with artist, album, and genre meta information⁴⁷; and the CiaoDVD dataset⁴⁸. By extracting data from each dataset, we constructed a rating matrix in which 20% of the elements were rated, unless otherwise specified. The numbers of users (rows) and items (columns) in the rating matrix are $n = 250$ and $m = 500$, respectively, and the number of features is set to half the number of users, that is, $k = n/2$, unless otherwise specified. For the learning process, which involved the execution of NBMF/NMF, we concealed 20% of the rated elements together with the unrated ones. To evaluate the performance, we used the root mean squared error (RMSE) of the rated elements.

$$\sqrt{\frac{1}{|\mathcal{D}|} \sum_{(i,j) \in \mathcal{D}} (v_{ij} - r_{ij})^2}, \quad (10)$$

where \mathcal{D} is the set of rated elements, and $|\mathcal{D}|$ is the number of rated elements. v_{ij} is user i 's rating for item j , and r_{ij} denotes the corresponding predicted rating.

In our experiments, we applied NBMF and NMF to the same rating matrix. To ensure a comprehensive evaluation, we divided the rated elements into five distinct sets and performed five trials, masking one set at a time. The average was calculated for five trials, unless otherwise specified.

Figure 1 shows a comparison of RMSE and computation time of NBMF and NMF for 10 epochs. Each epoch involves updating matrix W followed by updating matrix H . The data points represent the averages of RMSE and computation time at each epoch, with some error bars too small to be observed. Figure 1 shows that the RMSE decays faster in NBMF than in NMF for all the datasets. Although the difference in the RMSE at each epoch between NBMF and NMF was negligible, the difference among the datasets was remarkable. The difference among the datasets originates from the frequency distribution of the ratings in each dataset, as shown in Figure 4. As elaborated later, when the distribution was sharp and the variance was small, the RMSE tended to be small. In contrast, when the variance in the frequency was large, the RMSE was relatively large.

Filling rate dependence

The filling rate of a rating matrix, which is the proportion of rated elements, influences collaborative filtering. However, the filling rate dependence of the RMSE varied across the datasets, as shown in Figure 2. In Figure 2, the RMSE was calculated after 10 epochs and averaged over five trials.

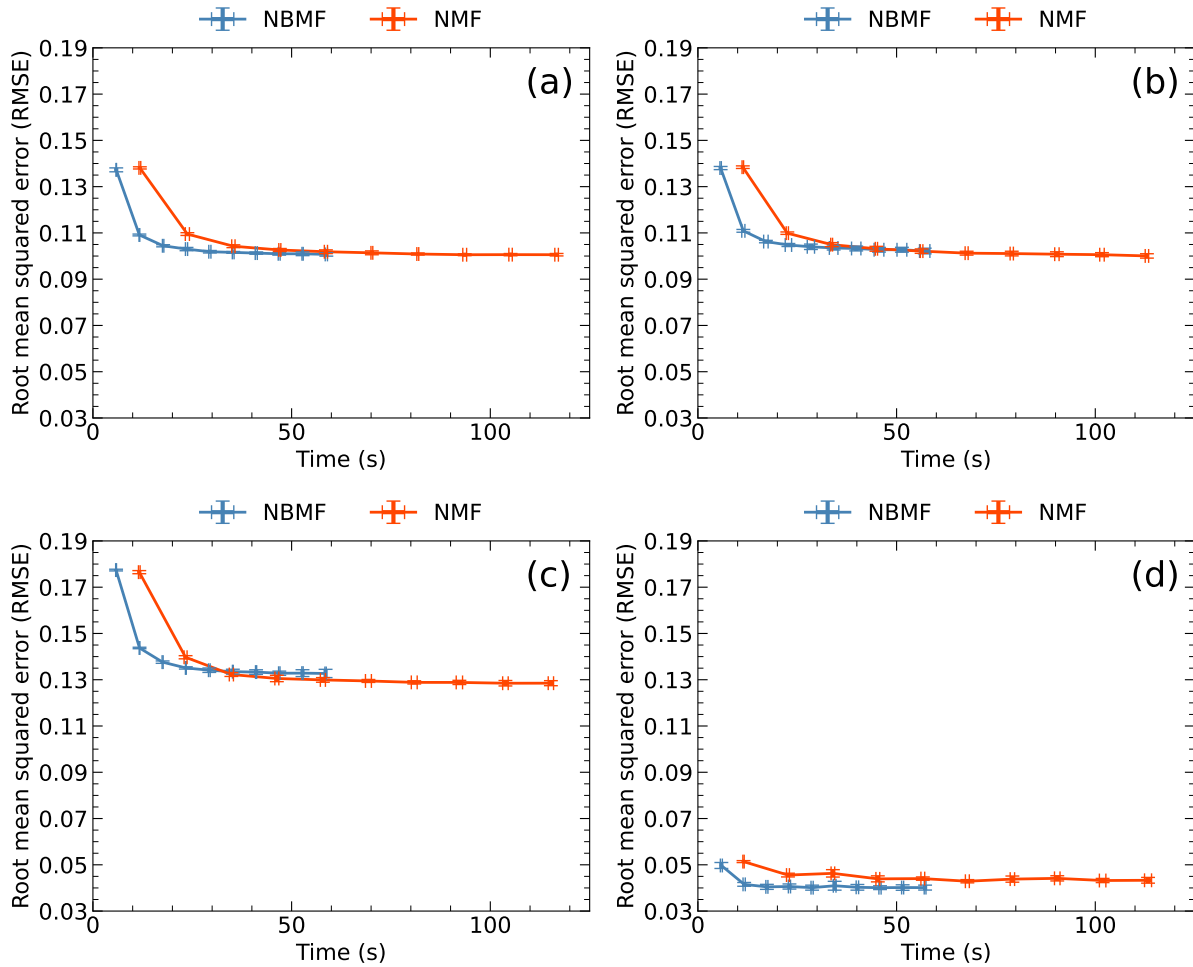


Figure 1. RMSE and computation time at each epoch, averaged over five trials, for (a) MovieLens, (b) Netflix, (c) Yahoo, and (d) CiaoDVD datasets. The error bars denote the standard deviation.

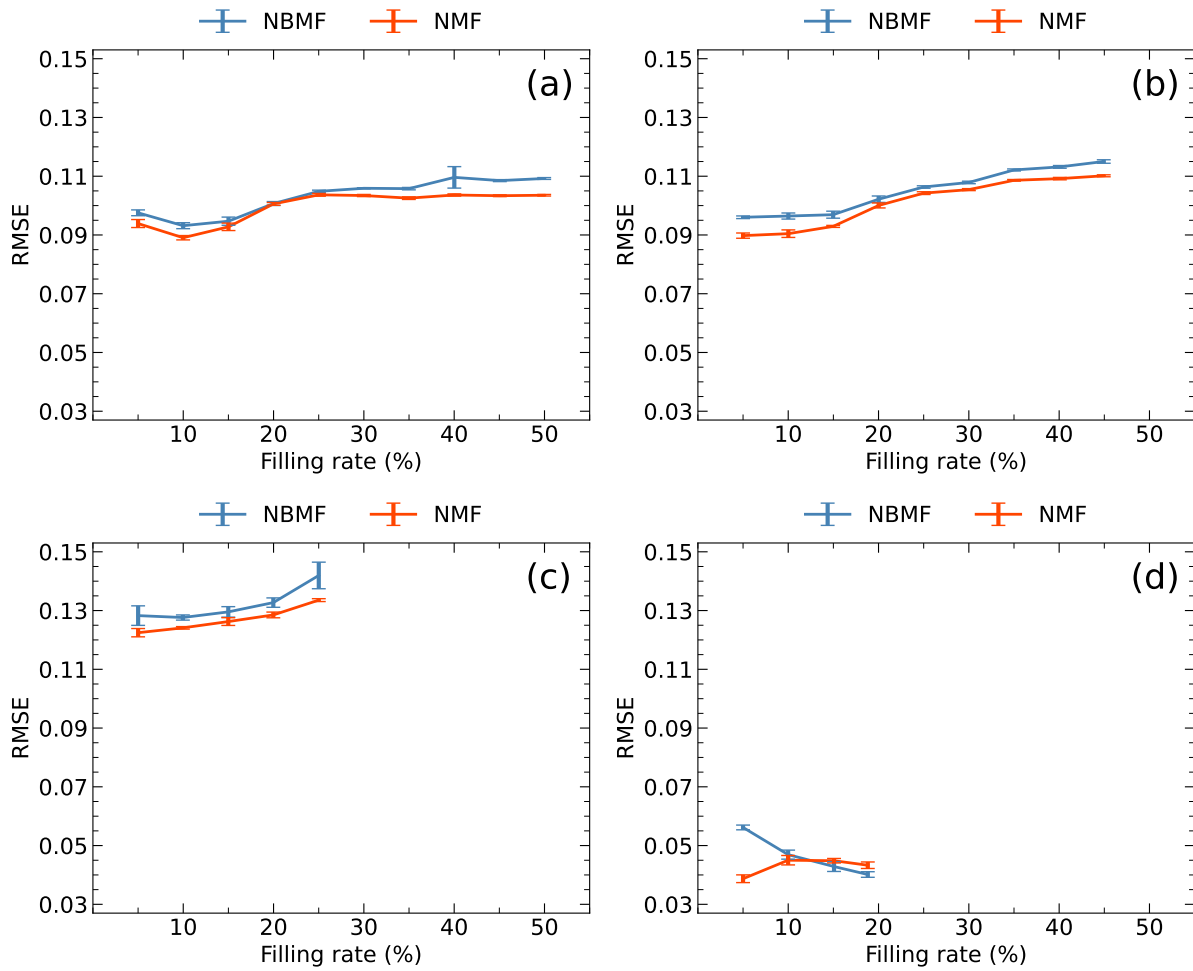


Figure 2. Filling rate dependence of RMSE for (a) MovieLens, (b) Netflix, (c) Yahoo, and (d) CiaoDVD datasets. Training data with filling rates more than 45%, 25%, and 20% could not be extracted for (b), (c), and (d), respectively. The data were averaged over five trials, with error bars denoting the standard deviation.

NMF is anticipated to yield lower RMSE values than NBMF owing to its higher resolution. However, in Figure 2a, the RMSEs for NBMF and NMF were comparable at the filling rate of approximately 20%. Furthermore, in Figure 2d, the RMSE for NBMF was smaller than that for NMF at the filling rate of approximately 20%. This inconsistent behavior suggests that the datasets differ significantly in their features.

Benefits of the masking procedure

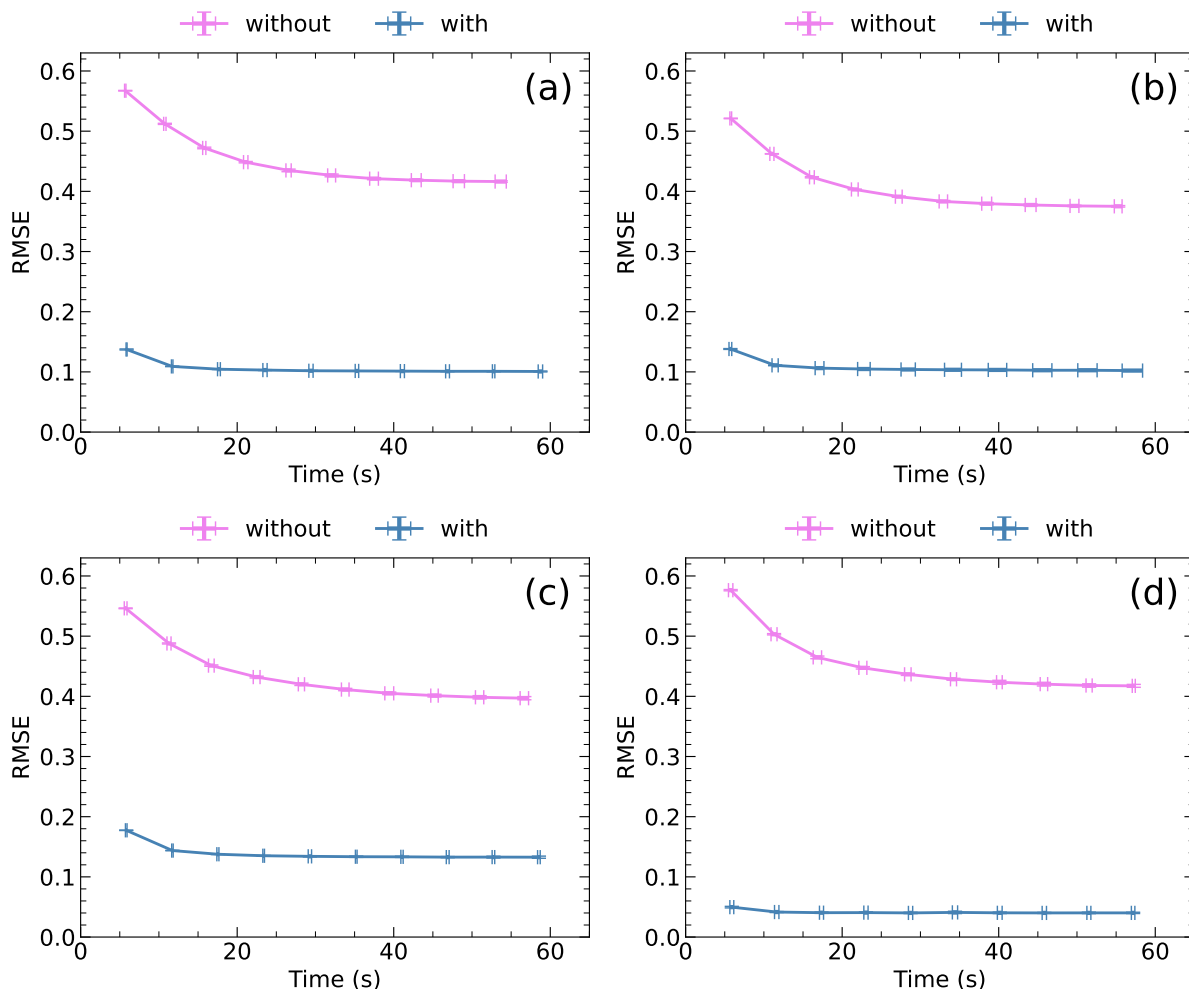


Figure 3. RMSE and computation time at each epoch with and without the masking procedure for NBMF for (a) MovieLens, (b) Netflix, (c) Yahoo, and (d) CiaoDVD datasets. The data were averaged over five trials, with error bars denoting the standard deviation.

Figure 3 shows the advantages of this masking procedure. The masking data for each dataset were the same as those used for NBMF in Figure 1. Notably, the RMSE without the masking procedure was about more than three times larger than the RMSE with the masking procedure for all the datasets. Furthermore, the difference in the computation time with and without the masking procedure was small. These findings indicate that the masking procedure offers apparent benefits in collaborative filtering, despite a minor drawback in terms of computation time.

Discussion and conclusions

The results indicate that the RMSE reflects certain properties of the data. Here, we focus on the frequency distribution of ratings, as illustrated in Figure 4. The distribution represents the percentage of ratings (1, 2, 3, 4, and 5) among the rated elements in a rating matrix, with a filling rate of 20%. The distributions in (a) and (b) showed a broad peak, and the corresponding RMSE had a similar value at 10 epochs in Figures 1a and 1b. However, the distribution in (c) showed two peaks at 1 and 5, leading to a large variance. The corresponding RMSE at 10 epochs in Figure 1c was larger than those of the other three data. By

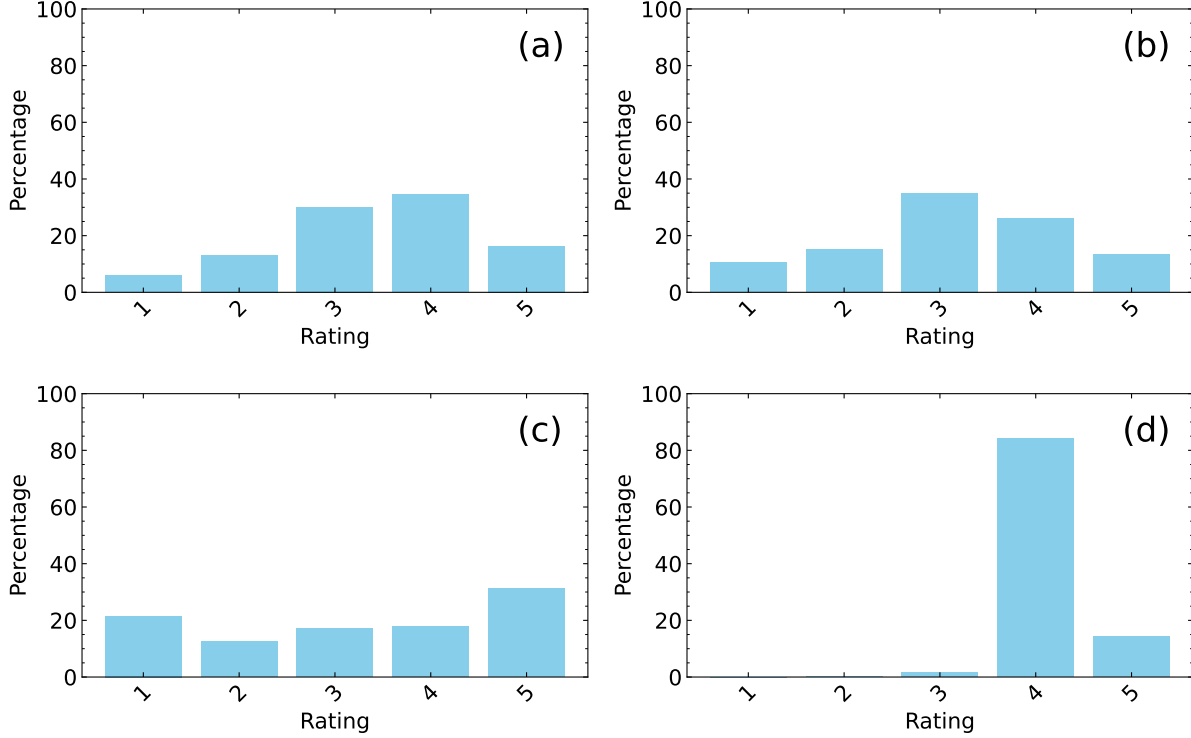


Figure 4. Frequency distributions of ratings expressed as percentages for (a) MovieLens, (b) Netflix, (c) Yahoo, and (d) CiaoDVD datasets.

contrast, the distribution in (d) had a steep peak at 4, indicating that more than 80% of the rated elements had a value of 4. The corresponding RMSE at 10 epochs in Figure 1d was significantly smaller than those of the other three data. This observation indicates that a distribution with a sharp peak and small variance typically results in a smaller RMSE. However, a distribution with a broader peak and larger variance often results in a larger RMSE.

The computation time for NBMF was significantly shorter than that for NMF under the same problem setup, as shown in Figure 5, for all the datasets. The total time required to update matrix W over 10 epochs was the same for both NMF and NBMF. However, the time required to update the matrix H in NMF was approximately six times longer than that in NBMF. This discrepancy suggests that the use of an SB-based machine accelerates the computation to update H . In fact, additional time is required to minimize Eq. (9) during the update of H . Executing minimization using the SB-based machine involves transforming the objective function into the Ising model form, as explained in the Methods section. Using the SB-based machine causes the communication time between the CPU and the FPGA, although it is a small fraction of the total time. Nevertheless, the overall computation time for NBMF, including these additional factors, was shorter than that for NMF.

Throughout this study, the ratio of the number of features to the number of users was fixed at $k/n = 0.5$. In general, the RMSE tends to decrease as the ratio increases. However, the computation time increases with the ratio because the matrix sizes of H and W increase. Therefore, a moderate value needs to be selected for this ratio. As shown in Figure 6, the rate of improvement in the RMSE was slow for the ratios of 0.5 or greater for all the datasets. Considering this result, we chose $k/n = 0.5$ as an appropriate value for this ratio.

Although our results support the computational advantages of NBMF, there are several limitations. Notably, the performance of NBMF is highly sensitive to the characteristics of datasets. NMF, which operates on continuous variables, exhibits comparable or superior accuracy in certain cases compared with NBMF. This is attributed to the higher resolution of continuous representations than binary ones. Furthermore, it is necessary to employ a low-latency system to realize the advantage of computation time. Even with a high-performance Ising machine, communication overhead between the CPU and the Ising machine can significantly impact overall performance. Therefore, utilizing a low-latency Ising machine is crucial for efficiently executing NBMF.

In summary, we proposed a novel approach that employs NBMF with masking for collaborative filtering, and our findings demonstrate a substantial improvement in the estimation performance as a result of the masking procedure. Moreover, our results highlighted the computational advantage of employing an SB-based machine in NBMF. NBMF with masking can be

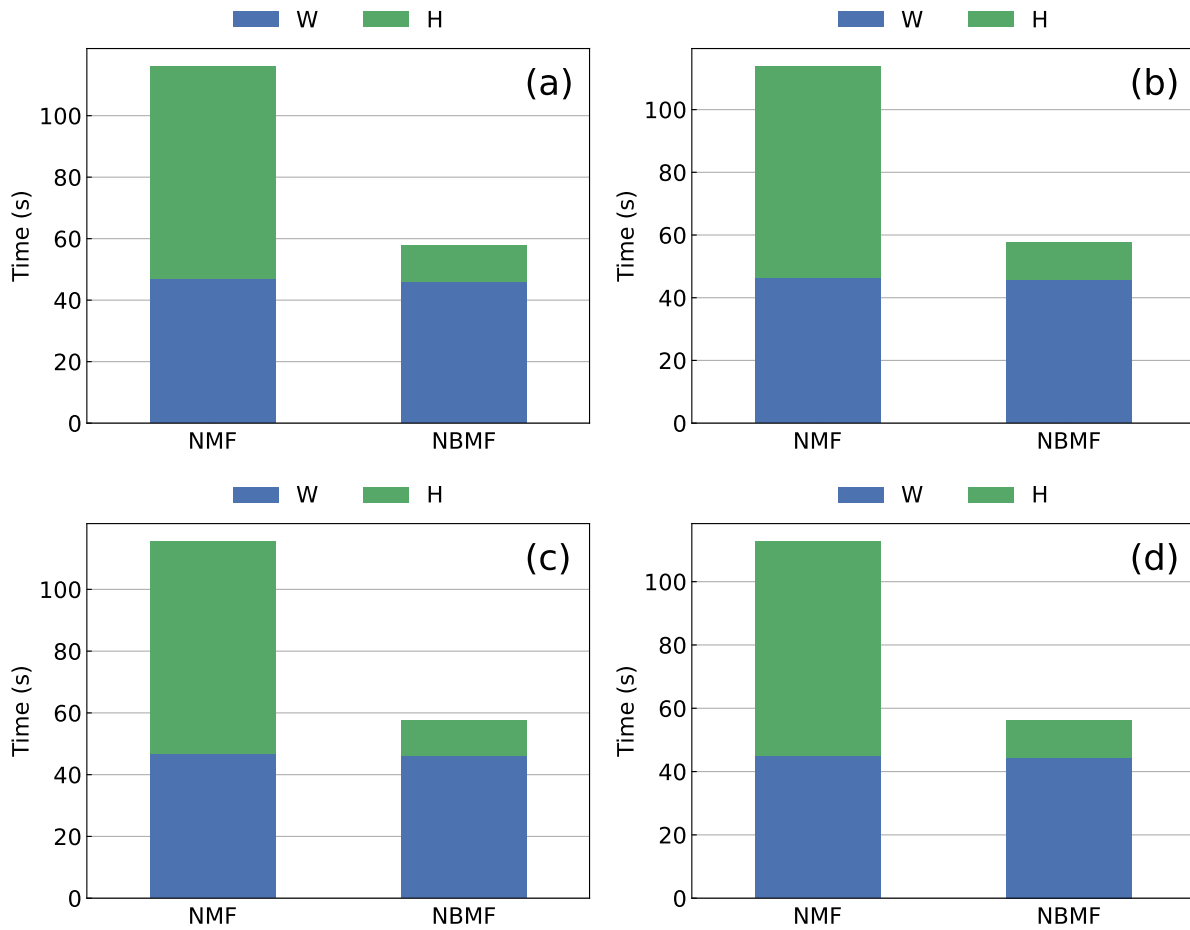


Figure 5. Computation time for 10 epochs in NBMF and NMF methods for the (a) MovieLens, (b) Netflix, (c) Yahoo, and (d) CiaoDVD datasets. The blue and green bars represent the total times spent on updating matrices W and H , respectively.

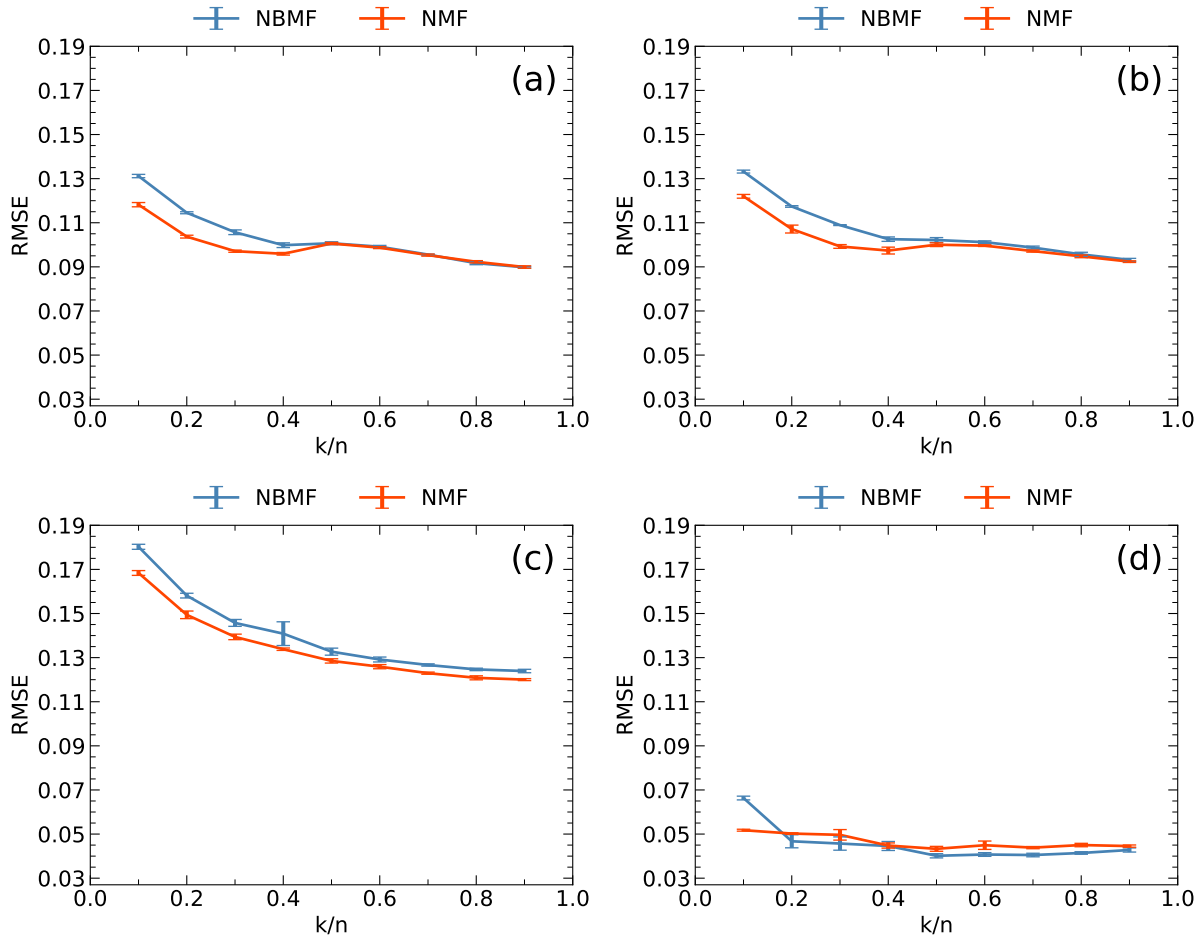


Figure 6. RMSE as a function of the ratio of the number of features k to that of users n for (a) MovieLens, (b) Netflix, (c) Yahoo, and (d) CiaoDVD datasets. The data were averaged over five trials, with error bars denoting the standard deviation.

applied in collaborative filtering across various datasets. This study reveals the potential of NBMF by utilizing an Ising machine for a wide range of applications.

Methods

Projected gradient method

The PGM⁵ for updating matrix W minimizes Eq. (4), and the gradient is given by

$$\nabla f_W = -H(\mathbf{v} - H^\top \mathbf{x}) + \lambda_1 \mathbf{x}. \quad (11)$$

The update rule for \mathbf{x} is given by

$$\mathbf{x}^{t+1} = P[\mathbf{x}^t - \gamma_t \nabla f_W(\mathbf{x}^t)], \quad (12)$$

where the projection is defined as

$$P[x_i] = \begin{cases} 0 & (x_i \leq 0), \\ x_i & (0 < x_i < x_{\max}), \\ x_{\max} & (x_{\max} \leq x_i). \end{cases} \quad (13)$$

In this study, we set $x_{\max} = 1$ as the upper bound of x_i . The learning rate γ_t was adjusted at each step t to satisfy the following inequality:

$$f_W(\mathbf{x}^{t+1}) - f_W(\mathbf{x}^t) \leq \sigma \nabla f_W(\mathbf{x}^t)^\top (\mathbf{x}^{t+1} - \mathbf{x}^t), \quad (14)$$

where $\sigma = 0.01$ in our experiments. Initially, we assigned γ_{t-1} to γ_t ($\gamma_0 = 1$). If γ_t satisfies Eq. (14), it is repeatedly divided by β , where we set $\beta = 0.1$ in our experiments, while the inequality holds. If γ_t does not satisfy Eq. (14), it is repeatedly multiplied by β until the inequality is satisfied. Following this adjustment, we calculated \mathbf{x}^{t+1} using Eq. (12). This procedure is repeated until $\|\mathbf{x}^{t+1} - \mathbf{x}^t\| \ll \varepsilon$, where $\varepsilon = 10^{-7}$ in our experiments.

Data preparation

The datasets used in this study were sparse, as shown in Table 1. The numbers of users and items presented in Table 1 are the dataset sizes imported for the calculation in this study. The filling rate, which is the proportion of rated entries, differs among the datasets. To compare the results of those datasets, we extracted data from the datasets to create a rating matrix with a specified filling rate.

Table 1. Dataset sizes (the numbers of users and items) and filling rates used in this study. The original sizes of the Netflix and Yahoo datasets are much larger: 480,189 users are on the Netflix dataset, and 1.8 million users are on the Yahoo dataset.

Dataset	Users	Items	Filling rate
MovieLens	6,040	3,706	4.47%
Netflix	432,229	1,406	1.15%
Yahoo	2,677	126,478	0.30%
CiaoDVD	21,019	71,633	0.11%

The method to extract data at a specified filling rate is as follows. First, we sorted the columns in the descending order of the percentage of filled elements in each column and then sorted the rows in a similar manner. Next, we selected an $n \times m$ matrix whose (1, 1) element coincides with the first-row and first-column element of the sorted table, and calculated the filling rate of the matrix. By shifting the (1, 1)-element location by one row and one column in the sorted table, we repeated the calculation of the filling rate. The $n \times m$ matrix whose filling rate was closest to the desired filling rate was selected as the rating matrix with the desired filling rate.

Ising formulation

The Ising machine (the SB-based machine in this study) seeks spin configurations that minimize the energy of the Ising model defined by

$$E = -\frac{1}{2} \sum_{i,j} J_{ij} s_i s_j + \sum_i h_i s_j. \quad (15)$$

Here, $s_i = \pm 1$ represents the i th spin, J_{ij} is the coupling coefficient between the i th and j th spins, and h_i is the local field on the i th spin. For minimizing Eq. (5), J_{ij} and h_i are given as follows:

$$J_{ij} = \begin{cases} -\frac{1}{2} \sum_r W_{ri} W_{rj} & (i \neq j), \\ 0 & (i = j), \end{cases} \quad (16)$$

$$h_i = \frac{1}{2} \left(\sum_r W_{ri} \left(\sum_j W_{rj} - 2u_r \right) + \lambda_2 \right). \quad (17)$$

To minimize Eq. (9) to update the j th row of $M \circ (WH)$, W_{rl} in Eqs. (16) and (17) are replaced with $(\tilde{W})_{rl} = M_{rj} W_{rl}$.

Simulated-bifurcation-based Ising machine

The SB algorithm, which is based on the adiabatic evolution in classical nonlinear systems that exhibit bifurcation, was introduced to accelerate combinatorial optimization^{23–25}. The SB algorithm has several variants, including adiabatic, ballistic, and discrete SB. In this study, we employed the ballistic SB method, whose update rule is described below²⁵.

$$y_i(t_{k+1}) = y_i(t_k) + \left\{ -[a_0 - a(t_k)]x_i(t_k) - \eta h_i + c_0 \sum_j J_{ij} x_j(t_k) \right\} \Delta_t, \quad (18)$$

$$x_i(t_{k+1}) = x_i(t_k) + a_0 y_i(t_{k+1}) \Delta_t, \quad (19)$$

where x_i and y_i are real numbers corresponding to the i th spin; a_0 , c_0 , and η are positive constants; and $a(t)$ is a control parameter that increases from zero to a_0 . The time increment is Δ_t ; thus, $t_{k+1} = t_k + \Delta_t$. After updating x_i at each time step, if $|x_i| > 1$, we replace x_i with $\text{sgn}(x_i) = \pm 1$ and set $y_i = 0$.

In our experiments, we employed a device with the FPGA implementation of the SB algorithm (SB-based Ising machine), the same one as in Ref. 26, to minimize Eqs. (5) and (9). The SB-based Ising machine (Figure 7) can solve fully-connected 2,048-spin Ising problems (the machine size M is 2,048), featuring a computational precision of 32-bit floating points and a system clock frequency of 259 MHz. As shown in Figure 7a, the FPGA (Intel Stratix 10 SX 2800 FPGA) on the board (Intel FPGA PAC D5005 accelerator card) is connected to a CPU (Intel Core i9-9900K, 3.60 GHz) via a PCIe bus (Gen 3×16, peak bandwidth of 15.75 GB/s). The NBMF process is executed using a CPU; however, the Ising problems described in Eqs. (16) and (17) are transferred/solved (offloaded) to/using the SB-based Ising machine. The computation times shown in Figures 1, 3, and 5 include the processing times of the CPU and FPGA and the data transfer times (overhead times) between them. The NMF process was executed only on the CPU (no data transfer time). The column update problems involved in updating the matrix H [Eq. (5)], each formulated as an Ising problem of size k [Eqs. (16) and (17)], are independent and thus can be processed simultaneously. By packing the multiple-column update problems as a large Ising problem, as shown in Figure 7b [placing the small J matrices on the diagonal line with zero padding to the remaining off-diagonal components], we solve $\lfloor M/k \rfloor$ column update problems simultaneously using the SB-based Ising machine with size M , where $\lfloor A \rfloor$ is the floor function of $A \in \mathbb{R}$.

Data Availability

Data supporting the findings of this study are available from the corresponding author upon request.

References

1. Herlocker, J. L., Konstan, J. A. & Riedl, J. Explaining collaborative filtering recommendations. In *Proceedings of the 2000 ACM conference on Computer supported cooperative work*, CSCW '00, 241–250, DOI: <https://doi.org/10.1145/358916.358995> (Association for Computing Machinery, New York, NY, USA, 2000).
2. Su, X. & Khoshgoftaar, T. M. A Survey of Collaborative Filtering Techniques. *Adv. Artif. Intell.* **2009**, e421425, DOI: <https://doi.org/10.1155/2009/421425> (2009).
3. Lee, D. D. & Seung, H. S. Learning the parts of objects by non-negative matrix factorization. *Nature* **401**, 788–91, DOI: <https://doi.org/10.1038/44565> (1999).
4. Lee, D. D. & Seung, H. S. Algorithms for non-negative matrix factorization. In *Proceedings of the 13th International Conference on Neural Information Processing Systems*, NIPS'00, 535–541 (MIT Press, Cambridge, MA, USA, 2000).
5. Lin, C. J. Projected gradient methods for nonnegative matrix factorization. *Neural Comput.* **19**, 2756–2779, DOI: <https://doi.org/10.1162/neco.2007.19.10.2756> (2007).

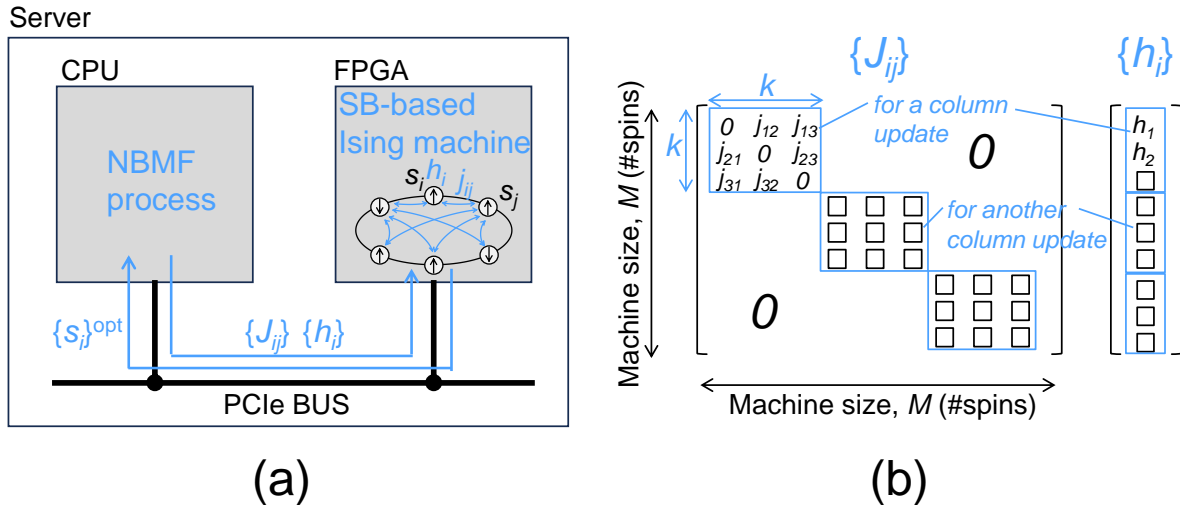


Figure 7. SB-based Ising machine. (a) System configuration. (b) Packing of multiple small Ising problems as a large Ising problem.

6. O'Malley, D., Vesselinov, V. V., Alexandrov, B. S. & Alexandrov, L. B. Nonnegative/binary matrix factorization with a D-Wave quantum annealer. *PLoS ONE* **13**, 1–12, DOI: <https://doi.org/10.1371/journal.pone.0206653> (2018).
7. Golden, J. & O'Malley, D. Reverse annealing for nonnegative/binary matrix factorization. *PLoS ONE* **16**, 1–10, DOI: <https://doi.org/10.1371/journal.pone.0244026> (2021).
8. Amin, M. H., Andriyash, E., Rolfe, J., Kulchytsky, B. & Melko, R. Quantum Boltzmann Machine. *Phys. Rev. X* **8**, 021050, DOI: <https://doi.org/10.1103/PhysRevX.8.021050> (2018).
9. Li, R. Y., Felice, R. D., Rohs, R. & Lidar, D. A. Quantum annealing versus classical machine learning applied to a simplified computational biology problem. *npj Quantum Inf.* **4**, 1–10, DOI: <https://doi.org/10.1038/s41534-018-0060-8> (2018).
10. Kitai, K. *et al.* Designing metamaterials with quantum annealing and factorization machines. *Phys. Rev. Res.* **2**, 013319 (2020).
11. Willsch, D., Willsch, M., De Raedt, H. & Michielsen, K. Support vector machines on the D-Wave quantum annealer. *Comput. Phys. Commun.* **248**, 107006, DOI: <https://doi.org/10.1016/j.cpc.2019.107006> (2020).
12. Asaoka, H. & Kudo, K. Image analysis based on nonnegative/binary matrix factorization. *J. Phys. Soc. Jpn.* **89**, 085001, DOI: <https://doi.org/10.7566/JPSJ.89.085001> (2020).
13. Nath, R. K., Thapliyal, H. & Humble, T. S. A Review of Machine Learning Classification Using Quantum Annealing for Real-World Applications. *SN Comput. Sci.* **2**, 365, DOI: <https://doi.org/10.1007/s42979-021-00751-0> (2021).
14. Asaoka, H. & Kudo, K. Nonnegative/binary matrix factorization for image classification using quantum annealing. *Sci. Reports* **13**, 16527, DOI: <https://doi.org/10.1038/s41598-023-43729-z> (2023).
15. Johnson, M. W. *et al.* Quantum annealing with manufactured spins. *Nature* **473**, 194–198 (2011).
16. Yamaoka, M. *et al.* A 20k-spin Ising chip to solve combinatorial optimization problems with CMOS annealing. *IEEE J. Solid-State Circ.* **51**, 303–309, DOI: <https://doi.org/10.1109/JSSC.2015.2498601> (2016).
17. Yamamoto, K. *et al.* A time-division multiplexing Ising machine on FPGAs. In *Proceedings of the 8th International Symposium on Highly Efficient Accelerators and Reconfigurable Technologies*, HEART2017 (Association for Computing Machinery, New York, NY, USA, 2017).
18. Kihara, Y. *et al.* A new computing architecture using Ising spin model implemented on FPGA for solving combinatorial optimization problems. In *2017 IEEE 17th International Conference on Nanotechnology (IEEE-NANO)*, 256–258 (2017).
19. Aramon, M. *et al.* Physics-inspired optimization for quadratic unconstrained problems using a digital annealer. *Front. Phys.* **7**, 48, DOI: <https://doi.org/10.3389/fphy.2019.00048> (2019).
20. Okuyama, T., Sonobe, T., Kawarabayashi, K.-i. & Yamaoka, M. Binary optimization by momentum annealing. *Phys. Rev. E* **100**, 012111, DOI: <https://doi.org/10.1103/PhysRevE.100.012111> (2019).

21. Matsubara, S. *et al.* Digital annealer for high-speed solving of combinatorial optimization problems and its applications. In *2020 25th Asia and South Pacific Design Automation Conference (ASP-DAC)*, 667–672 (2020).
22. Yamamoto, K. *et al.* Statica: A 512-spin 0.25M-weight full-digital annealing processor with a near-memory all-spin-updates-at-once architecture for combinatorial optimization with complete spin–spin interactions. In *2020 IEEE International Solid-State Circuits Conference - (ISSCC)*, 138–140 (2020).
23. Goto, H., Tatsumura, K. & Dixon, A. R. Combinatorial optimization by simulating adiabatic bifurcations in nonlinear hamiltonian systems. *Sci. Adv.* **5**, eaav2372, DOI: <https://doi.org/10.1126/sciadv.aav2372> (2019).
24. Tatsumura, K., Hidaka, R., Yamasaki, M., Sakai, Y. & Goto, H. A currency arbitrage machine based on the simulated bifurcation algorithm for ultrafast detection of optimal opportunity. In *2020 IEEE International Symposium on Circuits and Systems (ISCAS)*, 1–5 (IEEE, Seville, Spain, 2020).
25. Goto, H. *et al.* High-performance combinatorial optimization based on classical mechanics. *Sci. Adv.* **7**, eabe7953, DOI: <https://doi.org/10.1126/sciadv.abe7953> (2021).
26. Hidaka, R., Hamakawa, Y., Nakayama, J. & Tatsumura, K. Correlation-diversified portfolio construction by finding maximum independent set in large-scale market graph. *IEEE Access* **11**, 142979–142991, DOI: <https://doi.org/10.1109/ACCESS.2023.3341422> (2023).
27. Wang, Z., Marandi, A., Wen, K., Byer, R. L. & Yamamoto, Y. Coherent Ising machine based on degenerate optical parametric oscillators. *Phys. Rev. A* **88**, 063853, DOI: <https://doi.org/10.1103/PhysRevA.88.063853> (2013).
28. Marandi, A., Wang, Z., Takata, K., Byer, R. L. & Yamamoto, Y. Network of time-multiplexed optical parametric oscillators as a coherent Ising machine. *Nat. Photonics* **8**, 937–942 (2014).
29. Inagaki, T. *et al.* A coherent Ising machine for 2000-node optimization problems. *Science* **354**, 603–606, DOI: <https://doi.org/10.1126/science.aah4243> (2016).
30. McMahon, P. L. *et al.* A fully programmable 100-spin coherent Ising machine with all-to-all connections. *Science* **354**, 614–617, DOI: <https://doi.org/10.1126/science.aah5178> (2016).
31. Hamerly, R. *et al.* Experimental investigation of performance differences between coherent Ising machines and a quantum annealer. *Sci. Adv.* **5**, eaau0823, DOI: <https://doi.org/10.1126/sciadv.aau0823> (2019).
32. Pierangeli, D., Marcucci, G. & Conti, C. Large-scale photonic Ising machine by spatial light modulation. *Phys. Rev. Lett.* **122**, 213902, DOI: <https://doi.org/10.1103/PhysRevLett.122.213902> (2019).
33. Pierangeli, D., Marcucci, G., Brunner, D. & Conti, C. Noise-enhanced spatial-photonic Ising machine. *Nanophotonics* **9**, 4109–4116, DOI: <https://doi.org/10.1515/nanoph-2020-0119> (2020).
34. Pierangeli, D. *et al.* Adiabatic evolution on a spatial-photonic Ising machine. *Optica* **7**, 1535–1543, DOI: <https://doi.org/10.1364/OPTICA.398000> (2020).
35. Kang, Z., Peng, C., Yang, M. & Cheng, Q. Top-N Recommendation on Graphs. In *Proceedings of the 25th ACM International on Conference on Information and Knowledge Management, CIKM '16*, 2101–2106, DOI: [10.1145/2983323.2983649](https://doi.org/10.1145/2983323.2983649) (Association for Computing Machinery, New York, NY, USA, 2016).
36. Wang, D. *et al.* Elastic-net regularized latent factor analysis-based models for recommender systems. *Neurocomputing* **329**, 66–74, DOI: [10.1016/j.neucom.2018.10.046](https://doi.org/10.1016/j.neucom.2018.10.046) (2019).
37. Peng, C., Zhang, Z., Kang, Z., Chen, C. & Cheng, Q. Nonnegative matrix factorization with local similarity learning. *Inf. Sci.* **562**, 325–346, DOI: [10.1016/j.ins.2021.01.087](https://doi.org/10.1016/j.ins.2021.01.087) (2021).
38. Peng, C. *et al.* Log-based sparse nonnegative matrix factorization for data representation. *Knowledge-Based Syst.* **251**, 109127, DOI: [10.1016/j.knosys.2022.109127](https://doi.org/10.1016/j.knosys.2022.109127) (2022).
39. Wang, D. *et al.* A multi-view clustering algorithm based on deep semi-NMF. *Inf. Fusion* **99**, 101884, DOI: [10.1016/j.inffus.2023.101884](https://doi.org/10.1016/j.inffus.2023.101884) (2023).
40. Wang, D. *et al.* A generalized deep learning algorithm based on nmf for multi-view clustering. *IEEE Transactions on Big Data* **9**, 328–340, DOI: [10.1109/TBDATA.2022.3163584](https://doi.org/10.1109/TBDATA.2022.3163584) (2023).
41. Wang, D. *et al.* A Generalized Deep Learning Clustering Algorithm Based on Non-Negative Matrix Factorization. *ACM Transactions on Knowl. Discov. from Data* **17**, 99:1–99:20, DOI: [10.1145/3584862](https://doi.org/10.1145/3584862) (2023).
42. Deng, P. *et al.* Graph regularized sparse non-negative matrix factorization for clustering. *IEEE Transactions on Comput. Soc. Syst.* **10**, 910–921, DOI: [10.1109/TCSS.2022.3154030](https://doi.org/10.1109/TCSS.2022.3154030) (2023).

43. Wang, D. *et al.* DNSRF: Deep Network-based Semi-NMF Representation Framework. *ACM Trans. Intell. Syst. Technol.* **15**, 99:1–99:20, DOI: [10.1145/3670408](https://doi.org/10.1145/3670408) (2024).
44. Wang, D. *et al.* An autoencoder-like deep NMF representation learning algorithm for clustering. *Knowledge-Based Syst.* **305**, 112597, DOI: [10.1016/j.knosys.2024.112597](https://doi.org/10.1016/j.knosys.2024.112597) (2024).
45. Harper, F. M. & Konstan, J. A. The movielens datasets: History and context. *ACM Trans. Interact. Intell. Syst.* **5**, DOI: <https://doi.org/10.1145/2827872> (2015).
46. Netflix prize data. <https://www.kaggle.com/datasets/netflix-inc/netflix-prize-data>. (Accessed 1 October 2024).
47. Yahoo! music user ratings of songs with artist, album, and genre meta information, v. 1.0. <http://webscope.sandbox.yahoo.com>. (Accessed 1 October 2024).
48. Guo, G., Zhang, J., Thalmann, D. & Yorke-Smith, N. Etaf: An extended trust antecedents framework for trust prediction. In *Proceedings of the 2014 International Conference on Advances in Social Networks Analysis and Mining (ASONAM)* (2014).

Acknowledgements

This study was partially supported by JSPS KAKENHI (Grant Number JP23H04499) and Murata Science and Education Foundation.

Author contributions statement

Y.T. and Y.I. conceived and conducted the simulations and analyzed the results. Y.H. and K.T. discussed improvements in computing and parameter tuning. K.K. supervised the study and wrote the manuscript. All the authors reviewed the manuscript.

Additional information

Competing interests: K.T. is an inventor on a Japanese patent application related to this work filed by the Toshiba Corporation (no. P2019-164742, filed 10 September 2019). This study was conducted as collaborative research between Ochanomizu University and Toshiba Corporation. The authors declare that they have no other competing interests.